Planar Resonators for measurements of X-band EPR Spectra

A. Ghirri,[1, a)] G. Timco,[2] R. E. P. Winpenny,[2] and M. Affronte[3]

[1)] *Istituto Nanoscienze-CNR, via Campi 213/a, 41125 Modena (I).*

[2)] *School of Chemistry and Photon Science Institute, The University of Manchester, Oxford Road, M13 9PL, Manchester, UK.*

[3)] *Dipartimento di Scienze Fisiche, Informatiche e Matematiche, Universita di Modena e Reggio E. and Istituto Nanoscienze-CNR, via Campi 213/a, 41125 Modena (I)*

(Dated: 3 September 2014)

We fabricated planar Ag/Al_2O_3 microstrip lines and tested their application for continuous wave EPR spectroscopy of molecular magnets. We focused on a single-crystal of Cr_3 triangles and we made use of a X-band resonator to measure angle-dependent spectra at fixed frequency. We also tested a broadband transmission line to acquire spectra at varying frequency in the range 2-25 GHz. These results were used to extract the effective gyromagnetic factors for perpendicular directions, showing the presence of anisotropic interactions for the system under study.

PACS numbers: 76.30.-v, 75.50.Xx, 75.75.-c

Keywords: Planar microresonators; Small-volume EPR; Molecular magnets

[a)] Electronic mail: alberto.ghirri@nano.cnr.it.

Electron Paramagnetic Resonance (EPR) is a powerful spectroscopic technique widely used in Chemistry, Physics and Biology. Conventional spectrometers usually employ 3D cavities that are optimized for specific electromagnetic (e.m.) modes and transitions[1]. To date, a large variety of them has been developed for specific applications, including high and multi-frequency, pulses, ENDOR, etc. as well as coherent manipulation of quantum states by means of sequences of pulses[2]. Planar resonator have been proposed as an alternative approach for magnetic resonance experiments and different geometries, including stripline[3], microstrip[4–7], coplanar[8–10] and microcoils[11–14] have been studied in detail for both continuous wave (CW) and pulsed EPR. Similar resonators were also used for ferromagnetic resonance measurements[15–17] while superconducting analogs have been used in circuit-QED experiments with superconducting qubits and spin ensembles.[18] Microstrip and coplanar circuits find also widespread applications in telecommunications as filters and antennas. These devices are fabricated by microelectronic circuit technology, that allows flexibility of design and scalability. The possibility to concentrate the microwave field by adapting the resonator to samples with reduced dimensions, such as small crystals, nanostructures, films or metamaterials determines improved sensitivity, which for optimized devices is reported to be comparable, or even superior, to conventional spectrometers.[11–14] Another characteristic is their excellent conversion efficiency, which allows to generate strong microwave fields with reduced power and dissipation. Together with the small heat load, it allows to micro-resonators to be installed in cryogenic refrigerators to carry out EPR measurements at temperature below 1 K.[8]

In this letter we describe a simple set-up based on planar resonators installed in a commercial cryo-magnetic system and measured by means of Vector Network Analyzer (VNA). We have designed and fabricated different types of X-band resonators and microstrips and tested them with different molecular nanomagnets (crystals, powders and films). Our results demonstrate that this techniques is well suitable and flexible for the characterization and study of these materials. In this Letter, we focus on a set of measurements on a molecular Cr_3 single crystals that comprises 3 Cr^{3+} ions, each carrying a spin 3/2, coupled by antiferromagnetic exchange one to another to give two well defined doublets as ground state of the molecule [Fig. 2 (c)]. The performances and sensitivity of our microstrip is thus tested by measuring spectra for this anisotropic sample under different conditions.

Microstrip lines are constituted by a dielectric substrate, with a conducting strip de-

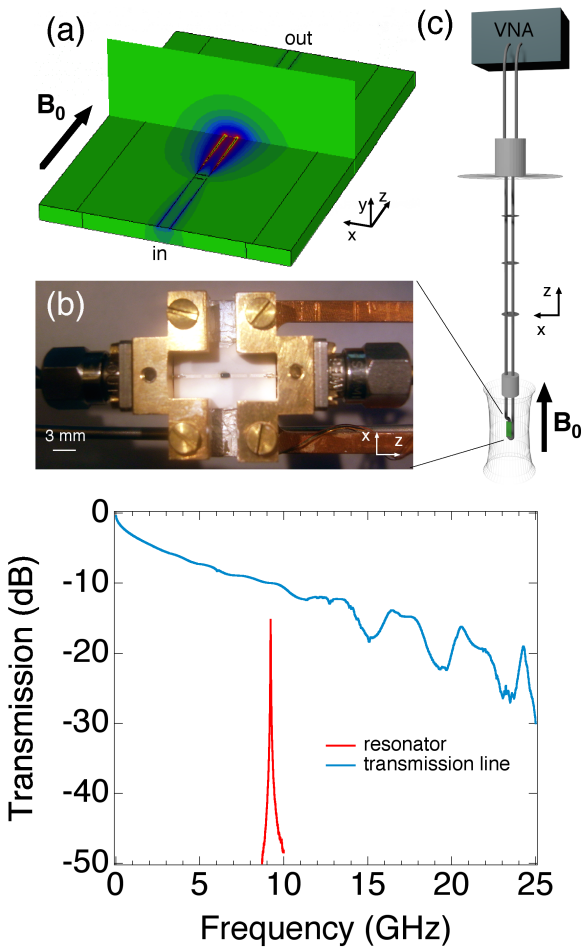

FIG. 1. (a) Finite element simulation of the averaged distribution of $|\mathbf{B_1}|$ of the X-band resonator. (b) Photograph of the Ag/Al_2O_3 resonator installed on the gold plated brass housing. A single-crystal of Cr_3 is visible at the center of the microstrip. (c) Schematic of the low temperature set-up. (d) S_{21}-vs-ν spectrum taken at $T = 2.5$ K for the bare resonator (red line) and the broadband transmission line (black line). Higher order harmonics of the resonator are not shown for clarity.

posited on top and a ground electrode on the bottom side.[19] For a given a substrate, having a known dielectric permeability and thickness, the width of the strip is calculated by standard methods to obtain a nominal impedance of 50 Ω. The transmission of an e.m. wave through the microstrip take place with a *quasi*-transverse mode, where the magnetic component $\mathbf{B_1}$ oscillates perpendicular to the central strip. We have studied two types of microstrip lines: The first is a simple microstrip of length 14 mm, which ideally displays broadband transmission without any resonances. The second type is a $\lambda/2$ X-band resonator, where

two gaps disconnect the central strip of length $l = 6$ mm from the feedlines. In this case, the size of l impose the resonance condition, that corresponds to the presence of a stationary wave at frequency $\nu_0 = \frac{c}{2\sqrt{\epsilon_{eff}}l}$, where $c = 3 \cdot 10^8$ m s^{-1} and ϵ_{eff} is the effective dielectric constant of the microstrip. Off resonance transmission is negligible. The width of the gap (δ) influences the insertion loss (IL) and the quality factor (Q) of the resonator. After a series of tests with different devices, we have chosen $\delta = 300$ μm because this value provided the lowest IL and the maximum Q on resonance.

We made use of finite element e.m. simulations (CST Microwave Studio) to calculate the distribution of the magnetic component of the microwave field. As expected for a $\lambda/2$ resonator, Fig. 1 (a) shows an antinode of $|\mathbf{B_1}|$ located at the center of the microstrip. Its maximum value (Supplementary Information) is slightly lower than that reported by Twig et al. for omega-type resonators.[14] The simulation carried out for the broadband device shows a traveling wave in place of a resonance. The maximum value of $|\mathbf{B_1}|$ calculated for the latter is approximately 10 times lower respect to that of the resonator. Besides of the possibility to span on different frequencies, the broadband line is thus expected to be less sensitive than the resonator.

Although different choices for dielectric and conductors are possible, we found good trade-off by fabricating silver microstrips by one-step optical lithography (lift-off) on 14x10x0.63mm^3 Al_2O_3 substrates ($\epsilon_r = 9.9$). 3 μm thick Ag film was thermally evaporated and post-annealed in vacuum at 400 C for 2 hours. This thickness allows to exceed the skin depth of silver in this frequency range ($\simeq 0.7$ μm). The microstrips were installed in a open housing made of gold plated brass [Fig. 1 (b)] that defines the ground and shields the resonator from the environment. The bottom side of the chip is glued to the base by means of silver paint, the central strip is instead glued to the pins of the two launchers placed at the opposite sides of the housing. The launcher connects pin and coaxial line through SMA connectors. The devices were initially tested at room temperature by connecting the SMAs directly to the calibrated ports of the VNA. Measurements were then carried out in vacuum and at low temperature, down to $T = 2.5$ K, in a commercial Quantum Design PPMS cryostat, by means of a dedicated insert wired with low thermal conductivity coaxial cables (Micro-Coax UT-085B-SS). These are thermalized by means of contact fingers to the sample chamber of the PPMS, and brought out of the cryostat, without interruptions, by means of two o-ring sealed vacuum feedthroughs [Fig. 1 (c)]. The microstrip is positioned at the center

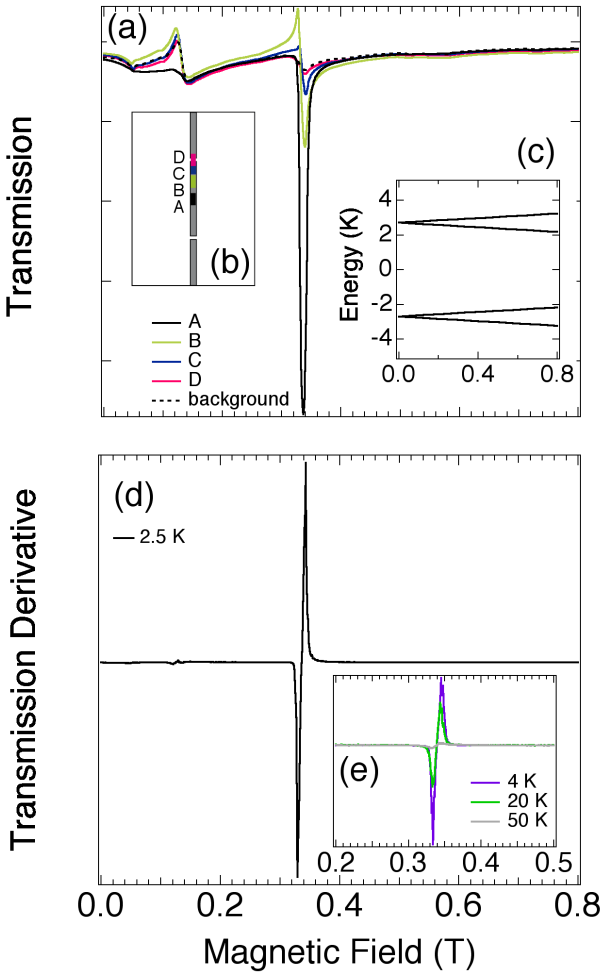

FIG. 2. (a) S_{21}-vs-B_0 CW spectra of the microstrip resonator with a single crystal of Cr_3 located in the positions indicated in (b) ($\theta = 0$, $T = 2.5$ K). The CW frequency is 9.215 GHz and it is shifted of -3 MHz respect to the bare resonator. (c) Plot of the lowest lying energy levels of the Cr_3 crystal as a function of B_0 ($\theta = 0$). The ground state is constituted by two doublets separated by an energy gap of few K. Detailed magnetic characterization will be reported elsewhere. (d) Numerical derivative of the transmission spectrum taken in the position A and (e) temperature dependence.

of the superconducting solenoid and oriented parallel to $\mathbf{B_0}$, thus the resonator operates in perpendicular EPR mode ($\mathbf{B_1} \perp \mathbf{B_0}$). The temperature is monitored by means of a calibrated ruthenium oxide thermometer positioned right on the back of the microstrip.

To characterize the frequency response of the devices we acquired reflection (S_{11}) and

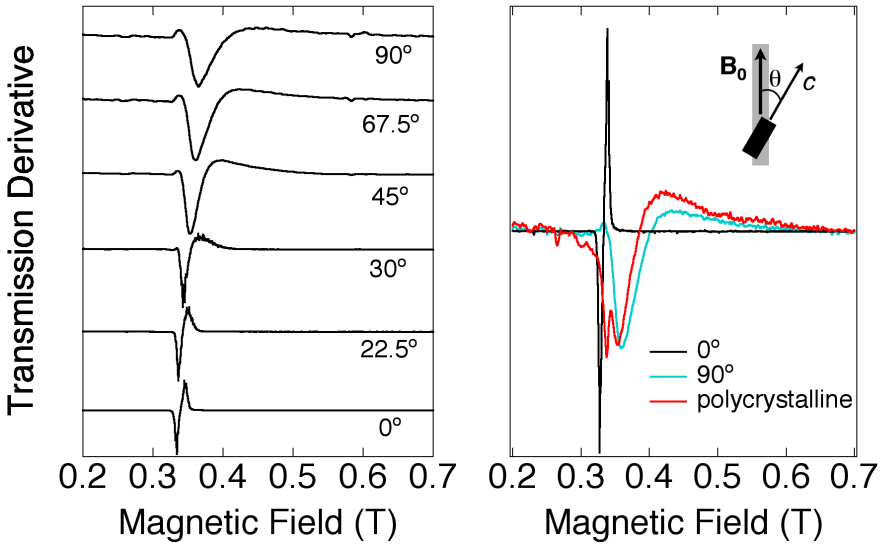

FIG. 3. (Left) Derivative of the transmission spectra measured at 2.5 K as a function of B_0 for different θ angles. For each spectrum the intensity is normalized to the maximum value. (Right) Comparison among the spectra taken at 0 and 90° and the spectrum of a polycrystalline sample. Inset. Definition of the θ angle comprised between $\mathbf{B_0}$ and the c-axis of the crystal.

transmission (S_{21}) spectra by means of our Vector Network Analyzer (Agilent PNA 26.5 GHz) operated with an output power of 10 mW. Fig. 1 (d) shows the comparison between the typical S_{21} spectrum of a resonator and a broadband line. The resonators (red line) show a well defined resonance in X-band (9.218 GHz in the case reported in Fig. 1), with quality factor exceeding 10^2 (typically 300-600). The S_{21}-vs-ν spectrum does not show dependence from the applied magnetic field and the Q factor is stable (Supplementary Information). The broadband transmission line (black line) shows instead, for $\nu < 10$ GHz, a monotone behavior for increasing frequency, with a progressive increment of the insertion loss ($IL = -S_{21}$ [dB]). For $\nu > 10$ GHz, due to the increase of the return loss ($RL = -S_{11}$ [dB]), some resonances occur (Supplementary Information). For both resonator and transmission line, S_{11} spectra are more affected by noise than S_{21} because of the effect of multiple reflections in the coaxial line. Thus, in the following we limit the discussion to transmission measurements.

The microwave absorption of the Cr_3 sample was evaluated by measuring S_{21} at fixed frequency while sweeping the applied magnetic field, in analogy to CW-EPR. Experimental data are obtained directly from the VNA that is a valid alternative to standard EPR set-up

with modulation coil and lock-in acquisition. mm-sized single crystals of molecular triangles of $Cr_3OPiv_6(H_2O)_3Piv$ were positioned directly above the central strip by means of a small amount of Apiezon N grease. The crystals have shape of hexagonal prisms and are indexed by X-ray diffractometry. The Cr_3 triangles lay parallel to the hexagonal face, hence with their perpendicular axis parallel to the c-axis of the crystal. We initially started with the single crystal oriented with $c||\mathbf{B_0}$ ($\theta = 0$) and we acquired the spectra with the crystal placed in different positions on the resonator (Fig. 2). We observed an absorption dip at 0.335 T which gets more intense as we move the crystal from the edge to the center of the resonator. The latter corresponds to the position where $\mathbf{B_1}$ is maximum, thus we assigned this feature to the magnetic dipole transition of the Cr_3 sample, determined by the presence of the ground state doublets [Fig. 2 (c)]. Conversely, the dip at about 0.12 T is visible also in the spectrum of the bare resonator, thus probably associated to the background of the cavity. In panel (d) we show the numerical derivative of the signal in pos. A after the subtraction of the background. The spectrum shows the characteristic line shape of a doublet transition with $g_{\|} = h\nu/\mu_B B_{\|} = 1.97$ ($h = 6.6262 \times 10^{-34}$ J s, $\mu_B = 9.2741 \times 10^{-24}$ J T^{-1} and $\nu = 9.215$ GHz). The temperature dependence of the peak is shown in panel (e) with a progressive decrease of the signal for increasing temperature.

To investigate the angular dependence of the absorption line at 0.335 T we performed a series of measurements by orienting the c-axis of the crystal at different angles θ respect to $\mathbf{B_0}$ (Fig. 3). The crystal was manually rotated and θ was measured under the microscope by means of a goniometer. The derivative of the transmission signal is shown in the left panel for different θ angles. As θ increases, the transition moves toward higher field and gets broader. For $\theta = 90°$ ($c \perp \mathbf{B_0}$) it is centered at about $B_{\perp} = 0.41$ T, thus the projection of the effective gyromagnetic factor in the plane of the ring is $g_{\perp} = h\nu/\mu_B B_{\perp} = 1.6$. The right panel displays also the comparison with the derivative signal taken for a polycrystalline sample of Cr_3. This spectrum shows multiple transitions in the same region, probably due to a weighted sum of the contributions given by the different orientations.

By means of the broadband transmission line we measured a series of CW spectra at different frequencies in the range 2-25 GHz. In this case, the absorption signal is weaker than that in Fig. 1, nevertheless it can be clearly distinguished from the background. In the upper panel of Fig. 4 we show a series of absorption dips taken at $\theta = 0$ and 22.5° and different frequencies. In the lower panel, the frequency of excitation is plotted as a function

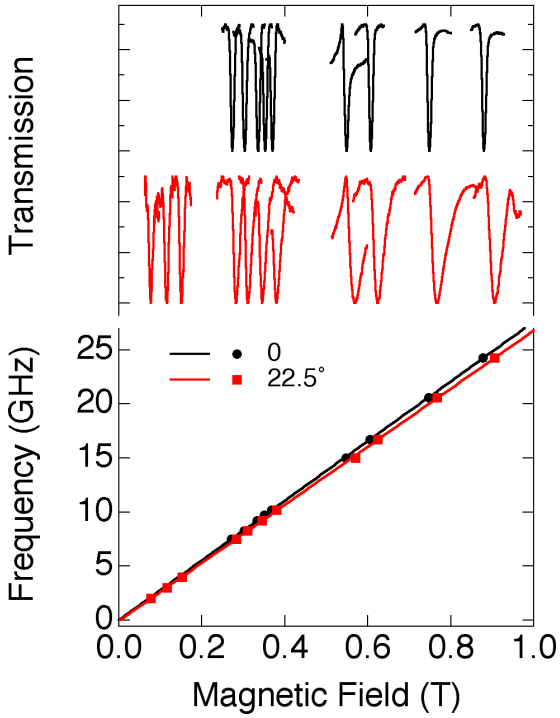

FIG. 4. Upper panel. Transmission spectra measured by means of the broadband microstrip for different microwave frequencies in the range 2-25 GHz and different orientations ($\theta = 0$, black; 22.5°, red). For each spectrum the intensity is normalized to the maximum value. Lower panel. Plot of the CW frequency as a function of the magnetic field correspondent to the absorption dip (markers). Solid lines represent the best fit with a linear function.

of the magnetic field of the transition. A linear behavior, well described by $\nu = g\mu_B B/\hbar$, is obtained. For $\theta = 0$ we used $g = g_{\|} = 1.97$ (black line in Fig. 4), while for $\theta = 22.5°$ (red line), $g = \sqrt{g_{\|}^2 \sin^2\theta + g_{\perp}^2 \cos^2\theta}$ with $g_{\perp} = 1.6$. This demonstrates that frequency dependence of resonances can be measured in this configuration at low temperature and applied magnetic field.

In conclusion, we fabricated and tested Ag/Al_2O_3 microstrips and we investigated their application for CW-EPR spectroscopy showing how they can be used to study a single-crystal of molecular magnets. We focused on Cr_3 molecular triangles and measured angle dependent EPR spectra to extract the gyromagnetic factors for perpendicular directions. These results point to the presence of anisotropic interactions, as assumed for other variants of Cr_3 clusters.[20] The approach we used is simple and versatile and can be applied for other

classes of materials or transitions (e.g. parallel-mode EPR). Reduction of the background signal can be achieved by using high purity substrates, such as sapphire. Thanks to their low heat capacity and their microwave conversion efficient with reduced dissipation, these devices are suitable for the installation on mK refrigerators and it will be also interesting to use this technique for pulsed experiments to study relaxation and decoherence.

We thank A. Cassinese for stimulating discussions, S. Ferrari for preliminary experiments and F. Vaccari for technical support. We also thank the Department of Engineering of the Universtity of Modena and Reggio E. for the CST simulations. This work was funded by FIRB project RBFR12RPD1 of the Italian Ministry of Research and by the US AFOSR/AOARD program, contract FA2386-13-1-4029.

REFERENCES

[1]J. A. Weil and J. R. Bolton, *Electron Paramagnetic Resonance*, 2nd ed. (Wiley, New York,, 2008) pp. pp. 21–23.

[2]K.-Y. Choi, Z. Wang, H. Nojiri, J. van Tol, P. Kumar, P. Lemmens, B. S. Bassil, U. Kortz, and N. S. Dalal, Phys. Rev. Lett. **108**, 067206 (2012).

[3]B. Johansson, S. Haraldson, L. Pettersson, and O. Beckman, Rev. Sci. Instrum. **45**, 1445 (1974).

[4]A. Torrezan, T. Mayer Alegre, and G. Medeiros-Ribeiro, Rev. Sci. Instrum. **80**, 075111 (2009).

[5]J. Henderson, C. Ramsey, H. Quddusi, and E. Del Barco, Rev. Sci. Instrum. **79**, 074704 (2008).

[6]J. J. Henderson, C. M. Ramsey, E. del Barco, T. C. Stamatatos, and G. Christou, Phys. Rev. B **78**, 214413 (2008).

[7]O. Benningshof, H. Mohebbi, I. Taminiau, G. Miao, and D. Cory, J. Magn. Reson. **230**, 84 (2013).

[8]P. Bushev, A. K. Feofanov, H. Rotzinger, I. Protopopov, J. H. Cole, C. M. Wilson, G. Fischer, A. Lukashenko, and A. V. Ustinov, Phys. Rev. B **84**, 060501 (2011).

[9]H. Malissa, D. Schuster, A. Tyryshkin, A. Houck, and S. Lyon, Rev. Sci. Instrum. **84**, 025116 (2013).

[10]C. Clauss, D. Bothner, D. Koelle, R. Kleiner, L. Bogani, M. Scheffler, and M. Dressel,

Appl. Phys. Lett. **102**, 162601 (2013).

[11]G. Boero, M. Bouterfas, C. Massin, F. Vincent, P.-A. Besse, R. S. Popovic, and A. Schweiger, Rev. Sci. Instrum. **74**, 4794 (2003).

[12]R. S. R. Narkowicz, D. Suter, J. Magn. Reson. **175**, 275284 (2005).

[13]R. Narkowicz, D. Suter, and I. Niemeyer, Rev. Sci. Instrum. **79**, 084702 (2008).

[14]Y. Twig, E. Suhovoy, and A. Blank, Rev. Sci. Instrum. **81**, 104703 (2010).

[15]G. Goglio, S. Pignard, A. Radulescu, L. Piraux, I. Huynen, D. Vanhoenacker, and A. Vander Vorst, Appl. Phys. Lett. **75**, 1769 (1999).

[16]F. Giesen, J. Podbielski, T. Korn, M. Steiner, A. Van Staa, and D. Grundler, Appl. Phys. Lett. **86**, 112510 (2005).

[17]Y. Liu, L. Chen, C. Tan, H. Liu, and C. Ong, Rev. Sci. Instrum. **76**, 063911 (2005).

[18]Z.-L. Xiang, S. Ashhab, J. Q. You, and F. Nori, Rev. Mod. Phys. **85**, 623 (2013).

[19]K. Gupta, R. Garg, I. Bahl, and P. Bhartia, *Microstrip Lines and Slotlines* (Artech House, Boston, 1996).

[20]A. Figuerola, V. Tangoulis, J. Ribas, H. Hartl, I. Brudgam, M. Maestro, and C. Diaz, Inorg. Chem. **46**, 11017 (2007).

I. SUPPLEMENTARY INFORMATION

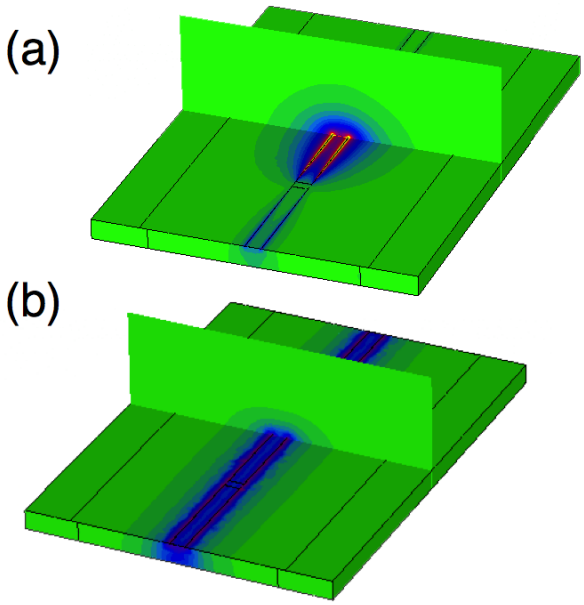

FIG. 5. Finite-element simulation of the phase-averaged value of $|\mathbf{B_1}|$ for (a) resonator and (b) broadband line. The vertical scale is 1000 A/m for (a) and 200 A/m for (b). The incident microwave power is 1 W.

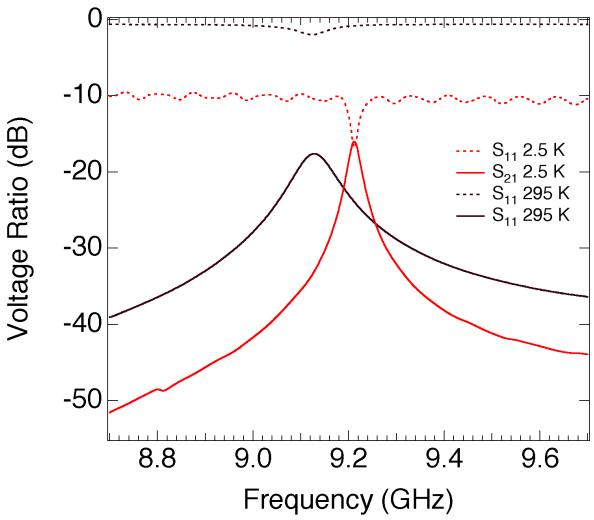

FIG. 6. Comparison between reflection (S_{11}) and transmission (S_{21}) frequency spectra measured at room temperature and 2.5 K. At room temperature, the device is measured directly at the VNA calibrated ports, here the quality factor obtained from S_{21} is $Q = 103$ and insertion loss $IL = 17.6$ dB. The spectra measured at 2.5 K show $Q = 354$ and $IL = 16.0$ dB. In this case an attenuation of 10 dB is introduced by the $\simeq 2$ m long coaxial line. The improvement of the insertion loss and Q-factor can be ascribed to the higher electrical conductivity at low temperature. The shift of the resonance frequency from room temperature to 2.5 K is of 85 MHz (0.01%).

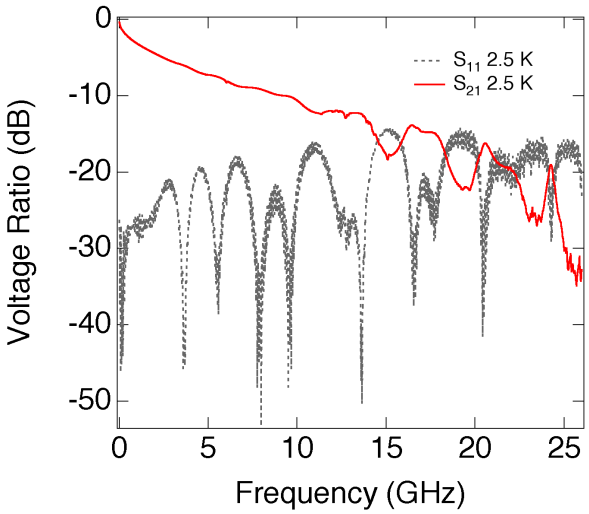

FIG. 7. S_{11} and S_{21} frequency spectra measured at 2.5 K for the broadband transmission line. For frequency $\nu < 10$ GHz, the S_{21} spectrum shows a monotone increase of the insertion loss. For $\nu > 10$ GHz, some resonance occur probably due to reflections at the contact points between microstrip and launchers.

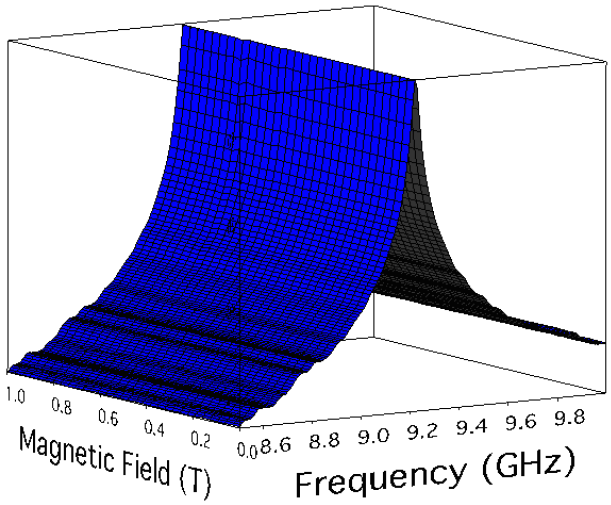

FIG. 8. S_{21}-vs-ν spectra measured for different magnetic fields for the X-band resonator. The resonance does not show field dependence and the Q factor for this resonator is stable and equal to 420.